ChemPhysChem

Chemistry Europe
European Chemical Societies Publishing

Reprint

WILEY-VCH

Raman Optical Activity of Glucose and Sorbose in Extended Wavenumber Range

Vladimír Palivec,[a] Pavel Michal,[b] Josef Kapitán,*[b] Hector Martinez-Seara,*[a] and Petr Bouř*[a]

Raman optical activity (ROA) is pursued as a promising method for structural analyses of sugars in aqueous solutions. In the present study, experimental Raman and ROA spectra of glucose and sorbose obtained in an extended range (50–4000 cm^{-1}) are interpreted using molecular dynamics and density functional theory, with the emphasis on CH stretching modes. A reasonable theoretical basis for spectral interpretation was obtained already at the harmonic level. Anharmonic corrections led to minor shifts of band positions (up to 25 cm^{-1}) below 2000 cm^{-1}, while the CH stretching bands shifted more, by ~180 cm^{-1}, and better reproduced the experiment. However, the anharmonicities could be included on a relatively low approximation level only, and they did not always improve the harmonic band shapes. The dependence on the structure and conformation shows that the CH stretching ROA spectral pattern is a sensitive marker useful in saccharide structure studies.

1. Introduction

Saccharides in solutions are challenging to study for many reasons. They are often very flexible, the OH groups may rotate and some five and six-membered rings pucker, which results in a presence of many conformers. Some species do not form crystals needed for x-ray diffraction. Because of their chemical structure and polarity, they strongly interact with water-rich environments.[1] They also usually lack a chromophore suitable for electron spectroscopy.[2] On the other hand, they are natural targets of vibrational optical activity (VOA), either in the form of vibrational circular dichroism (VCD)[3,4] or Raman optical activity (ROA),[5–7] where most of them provide useful spectral signals. These vibrational spectroscopic methods may also complement or verify NMR studies.[8,9] In this work, we focus on the rather unexplored ROA CH stretching pattern within ~ 2800–3100 cm^{-1}.

The ROA spectroscopy detects differential scattering of left and right circular polarized light. Its application to aqueous solutions of sugars is particularly convenient because Raman scattering of water is relatively weak and except for the OH stretching signal does not interfere with the measurement. Unlike in VCD, a wealth of characteristic spectral features is relatively easily detectable for most saccharide molecules.[10] The first ROA spectrometers were capable of measuring a wide range of vibrational frequencies (~100-3600 cm^{-1}), including the CH stretching.[11] However, later spectrometers exclusively focused on lower frequencies (approximately 200–2400 cm^{-1}), due to the limitations of the coupled charge device (CCD) detectors. This enabled access to most of the "fingerprint" vibrational bands of organic molecules. Higher frequencies, in particular the CH stretching signal, thus could not be routinely measured anymore. Only lately, the interest in a broader (~50–4000 cm^{-1}) wavenumber region was renewed due to the possibility to access it with multiple gratings[12] or dual detection channels.[13,14] At the same time, theoretical tools needed for accurate spectral simulations and interpretations became available. They allow for a consistent treatment of multiple sugar conformations, molecular polarity, and to some extent also estimation of the anharmonic corrections important for the CH stretching vibrations.[15–17] According to our knowledge, the ROA sugar CH stretching signal has never been reported and analyzed before.

We investigate it for two sugars, glucose and sorbose (Figure 1), available in both the D- and L-enantiomers. The enantiomers make it easier to test the reliability of the measurement. Ideally, they should provide ROA spectra of opposite sign, so called "mirror images".

For both sugars, the harmonic calculations lead to spectra reasonably comparable to experiment, once the calculated frequencies are scaled.[18] For sorbose, we also compute the anharmonic corrections to vibrational energies and spectral intensities. These more costly calculations are facilitated by the limited conformational freedom of this molecule. Sorbose in water exists almost exclusively (>98%) in the β-pyranose form.[19] Since several monosaccharide studies dealt in detail with the lower-frequency range (<2000 cm^{-1}),[7,18] we discuss this spectral part only briefly and focus on the CH stretching bands (around 3000 cm^{-1}). Reasonable agreement between the simulated and experimental spectra suggests that this high-frequency part is also useful and sensitive to molecular structure including conformation. The results thus may pave

[a] V. Palivec, Dr. H. Martinez-Seara, Prof. P. Bouř
Institute of Organic Chemistry and Biochemistry
Academy of Sciences
Flemingovo náměstí 2, 16610, Prague, Czech Republic
E-mail: hseara@gmail.com
bour@uochb.cas.cz
[b] P. Michal, Dr. J. Kapitán
Department of Optics
Palacký University Olomouc
17. listopadu 12, 77146, Olomouc, Czech Republic
E-mail: kapitan@optics.upol.cz

Supporting information for this article is available on the WWW under https://doi.org/10.1002/cphc.202000261

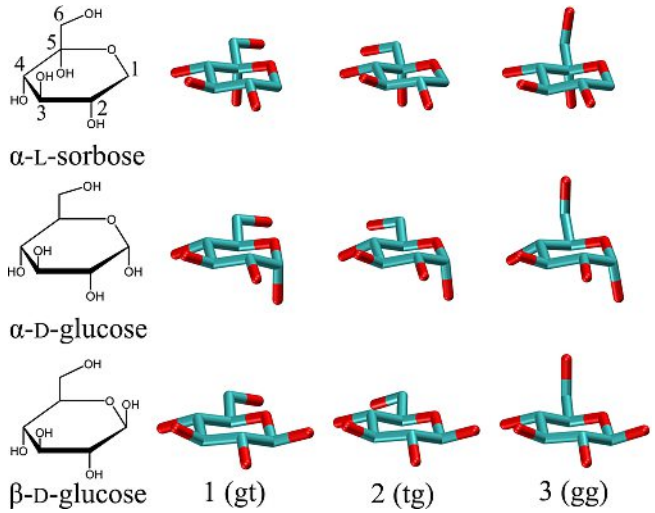

Figure 1. Studied molecules, α-L-sorbose, α- and β-D-glucose, and their three conformer classes (gauche-trans, trans-gauche and gauche-gauche, or 1, 2, 3) generated by the rotation of the exocyclic CH_2OH group. The standard carbon numbering is indicated for sorbose.

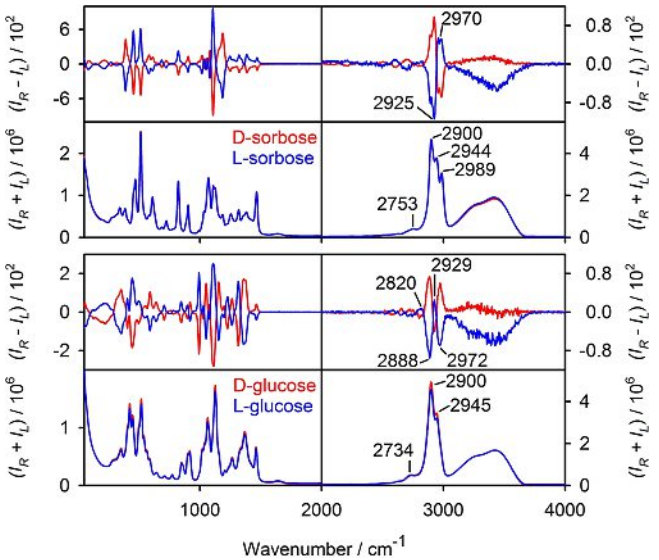

Figure 2. Experimental ROA ($I_R - I_L$) and Raman ($I_R + I_L$) spectra of sorbose and glucose enantiomers. Raman signal of water was subtracted, ROA baseline was not corrected. The ROA signal above 3000 cm^{-1} is not reliable because of instrumental artifacts associated with the strong Raman scattering of water. Intensity units are $cm \cdot J^{-1} \cdot mol^{-1} \cdot L$, sugar concentration was 2.6 mol/L.

the way for including this spectral region routinely in future saccharide studies, in a similar way as the more frequent fingerprint lower frequency range.

2. Results and Discussion

2.1. Experimental Spectra

The experimental ROA and Raman spectra of glucose and sorbose enantiomers in the whole wavenumber region available at the spectrometer (50–4000 cm^{-1}) are plotted in Figure 2. Below 3000 cm^{-1} the ROA bands exhibit excellent "mirror" symmetry, which proves the reliability of the measurement. Within the OH stretching region (~3020–3720 cm^{-1}), however, the ROA spectrum is hampered by instrumental artifacts.[10,20] These are caused by the high scattering of water (cf. Figures S1 and S2 in the Supporting Information with spectra without Raman baseline subtraction) and consequently low ROA/Raman intensity ratio (the so-called "circular intensity difference", CID < 2.5×10^{-6}).[21] Although the signal from the D- and L-sugar in this region differs, it cannot be trusted. In other words, ROA spectra of the OH stretching region are currently immeasurable. A weak Raman band at 2734 cm^{-1} may be most probably attributed to a combination or overtone CH bending vibration,[13,14] but its corresponding ROA is comparable to the noise.

On the other hand, the CH stretching ROA signal (~2800–3000 cm^{-1}) occurring below OH stretching band can be measured with a higher signal to noise ratio. Its CID is about 1.5×10^{-5}, which is still much less than for typical bands below 2000 cm^{-1} with CID ~5×10^{-4}, but it suffices for reliable recording.

For the L-sorbose enantiomer, ROA signal of the CH stretching mode comprises a strong negative band around 2925 cm^{-1} and a weaker positive one around 2970 cm^{-1}. Within 2500–2780 cm^{-1} at least three smaller bands appear in the Raman spectrum, attributable to a combination or overtone transitions. The region below 255 cm^{-1} up to the instrument limit around 50 cm^{-1} is also remarkable. While the Raman signal is monotonic, the ROA is far more structured. The overtone and the lowest-frequency vibrations, however, are difficult to interpret,[13] and their detailed analysis is planned for a separate study in the future.

The L-glucose CH stretching ROA intensity has about the same magnitude as for sorbose, but is more structured, with a weak positive band at 2820 cm^{-1}, and a "−+−" stronger band triplet at 2888/2929/2972 cm^{-1}. Similarly as for sorbose, weaker combination or overtone bands appear within ~2100–2780 cm^{-1}. Bellow 2000 cm^{-1}, the ROA spectrum has more balanced band intensities than for the sorbose. A weak ROA signal can also be seen close to the 50 cm^{-1} limit.

2.2. L-sorbose and D-glucose: High versus Low Frequency Region

In Figure 3 (top), we plot the simulated and experimental Raman and ROA spectra. The simulation is based on the harmonic model and MD cluster averaging, with conformer populations listed in Table 1. Although the instrument allows to express the spectra in absolute units ($cm \cdot J^{-1} \cdot mol^{-1} \cdot L$), this is currently inaccurate and for the analysis the calculated intensities are instead scaled to match the experiment.[18] When this scaling is done in the whole frequency range (top), the relative intensities do not match well: compared to the CH stretching the signal below 2000 cm^{-1} is smaller than in

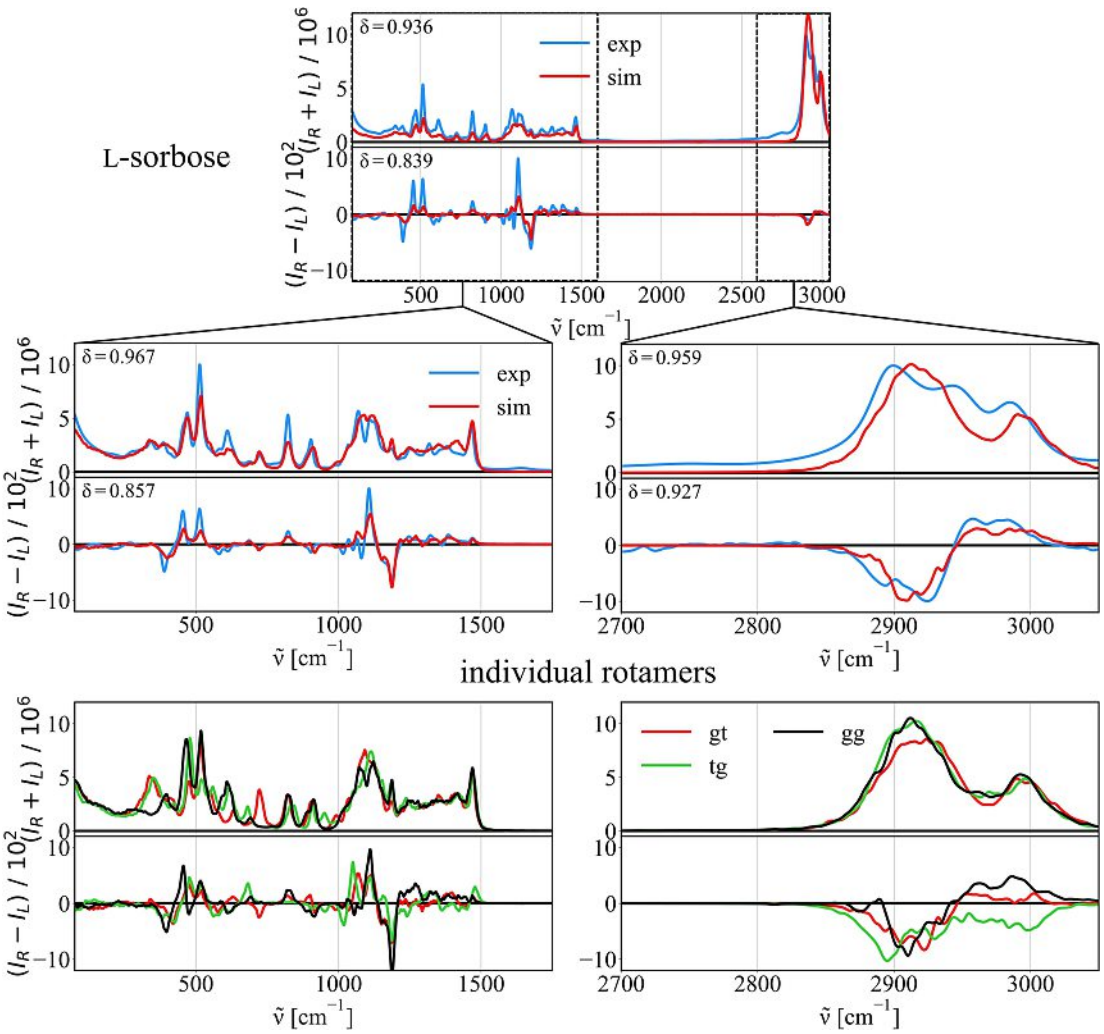

Figure 3. Experimental and simulated Raman and ROA spectra of L-sorbose (top), enlarged 75–1750 cm^{-1} and 2700–3050 cm^{-1} regions (middle), and theoretical spectra of individual gt, tg, and gg conformers (bottom). Conformer weights in the calculated spectra are listed in Table 1, see ref. [18] for harmonic frequency and intensity scaling procedures.

Table 1. *gt*, *tg* and *gg* ratios from MD (this work), anomer populations form ref. [24].

	p [%]			
	gt	*tg*	*gg*	anomer
sorbose	54	3	43	100
α-glucose	13	1	22	36
β-glucose	27	8	29	64

experiment. More reasonable results are obtained when the high- and low-frequency regions are treated separately (Figure 3, middle). Detailed discussion of region below 2000 cm^{-1} for monosaccharies, including the mode assignment, can be found elsewhere.[5,7,18] Most relative intensities and ROA band signs are predicted correctly. Occasional inconsistencies can be related to the DFT approximation, incomplete solvent model, or basis set.[7,18,22,23]

For the CH stretching signal, the agreement between the computed and experimental Raman and ROA intensities is about the same as for the vibrations below 2000 cm^{-1}. The intensity ratio between the lower (~2920 cm^{-1}) and higher (~2989 cm^{-1}) frequency Raman peaks is somewhat bigger in the simulation than in experiment, which can be explained by a fine vibrational mode splitting and coupling, not reproduced by the computation. In experiment, two bands (2900 and 2945 cm^{-1}) appear instead of the ~2920 cm^{-1} predicted one. The basic "−/+" (~2925/2970 cm^{-1}) ROA sign pattern is also reproduced by the simulation. Visual inspection of the normal mode movement allows one to estimate ranges where the CH stretching modes occur (Table 2); for individual conformers these are mostly spread over a wide frequency interval due to the OH group rotation and interaction with water. Individual MD snapshot (not shown) provided spectra very different from the average, similarly as for the fingerprint region of monosaccharides studied previously.[18] The CH_2 units seem to be least affected by the conformational changes, symmetric and asymmetric modes of which lie at the low- and high-frequency edges of the main CH stretching Raman and ROA signal.

Table 2. Calculated (Harmonic, Scaled) CH Stretching Frequencies.[a]

Frequency [cm^{-1}]	Assignment
2830–2910	$^{6}CH_2$ (locally) symmetric
2850–2945	CH
2900–2920	$^{1}CH_2$ symmetric
2910–2950	$^{6}CH_2$ asymmetric
2980–3030	$^{1}CH_2$ asymmetric

[a] Carbon numbering in Figure 1.

As seen from the conformer spectra (Figure 3, bottom) the Raman CH stretching signal does not depend much on the CH_2OH group rotation; in particular *gg* and *tg* are practically indistinguishable. This contrasts with the low-frequency region, where the conformational changes cause visible shifts/intensity changes in many bands. A similar observation was reported for the Ala-Ala dipeptide, where the CH stretching Raman signal did not depend much on the peptide conformation.[14] Unlike Raman, the CH stretching ROA spectrum is sensitive to conformational changes. For sorbose, it is clear that the *gg* conformer must be present in the sample as it is largely responsible for the positive 2970 cm^{-1} experimental signal.

The observations and conclusions made for sorbose are consistent with the results for glucose. The experimental spectra are compared with the theory in Figure 4. Also here the simulation well-reproduces CH stretching Raman intensities. As in experiment, the calculated glucose spectrum in the CH stretching region is less structured than for sorbose because of the anomeric equilibrium and consequent averaging of more variable conformers. The simulation provides somewhat less structured Raman CH stretching signal (one broad band) than observed (two close bands).

The CH stretching ROA of glucose is more structured than for sorbose, with a four band "2820(−)/2888(+)/2929(−)/2972 (+) cm^{-1}" experimental pattern. The computed spectrum reproduces this almost perfectly, only the lowest-frequency ~2820 cm^{-1} band is stronger and shifted to 2840 cm^{-1}.

Raman spectra of the α and β glucose anomers are predicted to be rather different below 2000 cm^{-1}. The Raman CH stretching is not much sensitive to the conformation including anomerization, only the *gg* rotamers seem to provide somewhat distinct spectra (Figure 4, bottom). The ROA, again, is very variable and clearly sensitive both to the CH_2OH rotation and the anomeric state.

2.3. Anharmonic Corrections

So far, the relatively good agreement of the calculations with the experiment was partially given by the harmonic frequency scaling (ref. [18] Experimental Section). This is consistent with a previous study,[14] where the anharmonic potential terms were found to be much more dependent on the conformation than the harmonic ones, and partially canceled during the averaging/molecular motion.

However, the raw (unscaled) harmonic CH stretching frequencies are too high, and the anharmonic computation provides values much closer to the experiment (Figure 5). Alternative comparison of the harmonic and anharmonic performance with scaled harmonic frequencies is shown in Figure S5. Unfortunately, the Raman and ROA band shapes, most indicative of the structure, are not always improved. One reason is that due to the convergence problems and other issues the anharmonic approach could not be pursued at the same level as the harmonic one (model I – "hybrid"). The anharmonic effects for Figure 5 were thus evaluated for the *gt*/*gg* (*0.56/0.44)* conformer mixture of L-sorbose (the *tg* conformer was neglected), using the "charges" solvent model (number III, see Methods).

A more detailed look at Figure 5 reveals that there are only minor differences in relative band intensities and ROA signs in the low-frequency region due to the anharmonic corrections. They cause only small frequency shifts (from 0 to 25 cm^{-1}), without changing the order of the vibrations. Within 1000–1300 cm^{-1}, the anharmonic frequencies are too low if compared to the experiment, and the harmonic ones are better. This can be attributed to the approximate character of the anharmonic method.[17]

The CH stretching is obviously affected more by the anharmonic corrections, with the harmonic frequencies shifted down by ~180 cm^{-1}, thus almost perfectly matching the experiment. However, the ratio of the main Raman bands (harmonic 3060/3047 cm^{-1}, Figure 5, or experiment 2900/2989 cm^{-1}, Figure 2), which is experimentally about 2:1, is more realistically obtained with the harmonic approach. Neither for ROA the anharmonicities clearly improve the harmonic CH stretching band shapes, at least at the level of the visual comparison.

Therefore, we can conclude with a mix message that the anharmonic corrections are certainly desirable, but at the present stage it is much more efficient and reasonably accurate to interpret the spectra using the harmonic approach, optionally combined with frequency scaling. Difficulties associated with the anharmonic treatment include not only the higher computational cost per snapshot (about 250-times longer time), but also a larger number of snapshots needed for converged spectra (~250 harmonic snapshots vs. at least 500 anharmonic ones per conformer).

2.4. Solvent Models

Finally, we compare the "hybrid" and "QM" solvent models for L-sorbose. The "hybrid" one is computationally significantly cheaper and has been already promoted for interpretation of the ROA sugar spectra in the lower-frequency range (200–1800 cm^{-1}).[18] In Figure 6 we can see that the two models give very similar results indeed. Some details are better reproduced by the QM model, such as relative intensity ratio of the Raman and ROA bands around 500 cm^{-1} and broader Raman signal around 2910 cm^{-1}. On the other hand, the hybrid model better

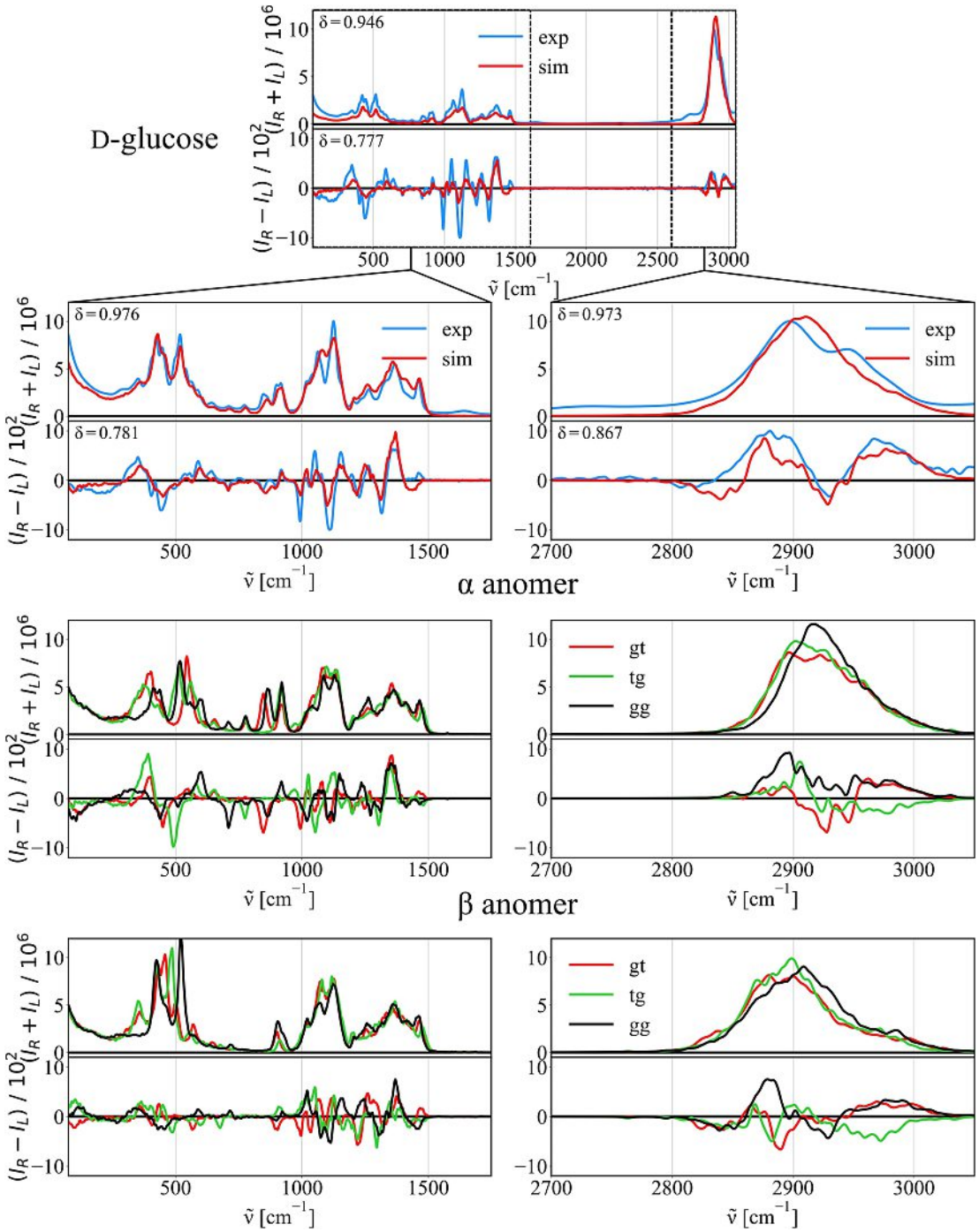

Figure 4. D-glucose, experimental and simulated Raman and ROA spectra (top panel), zoomed 75–1750 cm^{-1} and 2700–3050 cm^{-1} regions (below), and calculated spectra of individual conformers for the α and β anomers (lower half of the figure). As for Figure 3, conformer weights from Table 1 were used and harmonic frequencies and intensities scaled.[18]

reproduces fine features of ROA signal around 1300 cm^{-1}, or the shape of ROA signal around 2910 cm^{-1}.

3. Conclusions

The dual detection channel enabled us to measure high-quality Raman and ROA spectra of the D- and L-enantiomers of sorbose and glucose in a wide 50–4000 cm^{-1} frequency region. In the spectral analysis based on the combined MD and DFT computations, we focused on the CH stretching region. Its

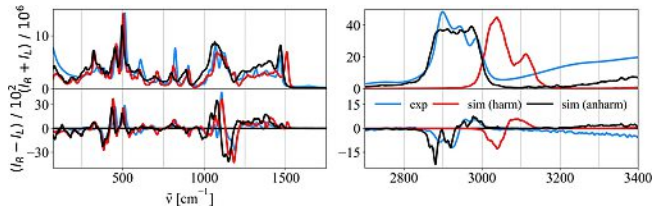

Figure 5. Harmonic and anharmonic Raman and ROA spectra of L-sorbose vs. experiment. Calculated frequencies are not scaled, the *gt/gg* ratio = 56/44 and the "charges" solvent anharmonic model were used.

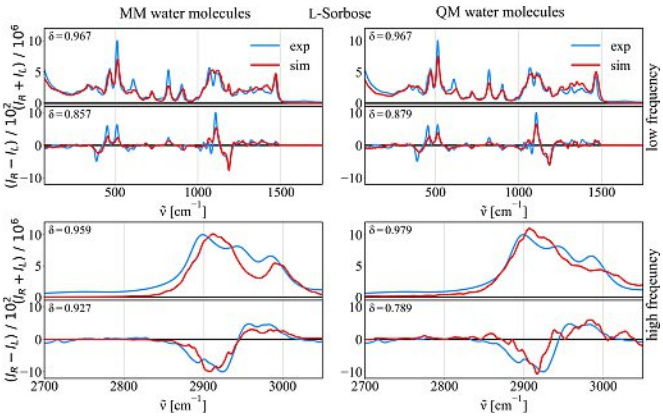

Figure 6. Raman and ROA spectra of L-sorbose calculated with two solvent models, using "MM water molecules" (model I – hybrid) and "QM water molecules" (model II – QM), as compared to the experiment.

sensitivity to the molecular conformation promises an additional spectroscopic marker to be used in future structural studies of saccharides. The simulations based on the harmonic approximation reproduced all the main spectral features including the CH stretching Raman and ROA intensity patterns. The anharmonic corrections via the generalized perturbation approach[16,17] applied for sorbose provided much more realistic vibrational frequencies; however, they somewhat destroyed the intensity patterns. Clearly, future improvements in the theoretical models are required for a more quantitative recovering and analysis of the experimental spectra. Nevertheless, even at present, the theory is already able to estimate the role of the solvent and the sugar conformational dependence, thus enabling to deduce the CH_2OH conformer and α/β anomer ratios. The measurement and analysis of the spectra in the extended wavenumber range will significantly increase the ROA potential for saccharide structural analyses.

Experimental Section

Raman and ROA Spectra Measurement

L- and D-enantiomers of sorbose and glucose (Figure 1) were obtained from Carbosynth and Sigma-Aldrich, respectively. The spectra were acquired on an ROA instrument constructed at the Palacký University, Olomouc, based on the design of W. Hug.[20,25] In addition to the original setup, zero-order light from the diffraction grating was used as a second detector channel, which made it possible to expand the measuring range, covering wavenumbers from 50 to 4000 cm^{-1}.[13,26] The sugars were dissolved in deionized water to two concentrations, 1.2 and 2.6 mol/L. Both of them provided very similar spectra (Figures S3 and S4); the higher concentration results with better signal to noise ratio are used in the main text. The samples were measured in a rectangular fused silica cell of 70 µl volume at 293 K, using back-scattering geometry, scattered circular polarization (SCP) modulation scheme,[10] Nd:YAG laser with 532 nm excitation wavelength, 0.7 W laser power at sample, and 10–30 h accumulation times. Water signal was subtracted from Raman spectra (cf. Figures S1 and S2). The intensities were calibrated with a tungsten-halogen lamp, normalized to unit molar concentration, and a minor (third-order five point Savitzky-Golay) smoothing was applied. They are plotted in counted photo-electrons per wavenumber per excitation energy per molar concentration (cm·J^{-1}·mol^{-1}·L).

Molecular Dynamics

MD simulations were performed using the Gromacs 2016 program package patched with Plumed.[27] One sugar molecule in $^4C_1$ chair conformation was placed in a 3^3 nm^3 cube, filled with water molecules. Previous studies showed that for these sugars the chair conformation remains relatively rigid and populations of other ring conformers are negligible.[5,18] The simulations were preformed using the *NpT* ensemble at 300 K and 1 bar, using the Nose-Hoover thermostat (1 ps^{-1} coupling constant)[28] and Parrinelo-Rahman barostat (1 ps^{-1} time constant and 4.5×10^{-5} bar^{-1} compressibility),[29] an *NpT* ensemble, and 2 fs integration time step. The Glycam-06 h[23] by means of the do-glycam software[30] and OPC3[31] force fields were used for the sugars and water, respectively. Hydrogen-containing bonds were frozen using the linear constraint solver.[32] For the search of neighboring atoms we used the Verlet list algorithm providing a pair list with buffering. One nm cutoffs were used both for the real part in the particle mesh Ewald method[33] and for van der Waals interactions, with a long range dispersion corrections for energy and pressure; van der Waals potentials were shifted to zero at the cutoff.

Equilibrium geometries of the three CH_2OH conformers (*tg*/*gt*/*tt*, Figure 1, Table 1) were determined MD simulations. For each conformer, a 5 ns constrained MD (restraining CH_2OH dihedral in found minima) was run, extracting either 250 or 500 snapshots (20 or 10 ps sampling rate) for the subsequent harmonic and anhamonic Raman/ROA calculations respectively. For sorbose, the α-anomer was neglected, as its structural contribution is negligible ($<2\%$) which did not alter the calculated spectra.[9,34] For glucose, however, both anomers are significantly populated, and the experimental α/β anomer ratio was used in spectral averaging.[35]

Solvent Models and Density Functional Theory

Using the MD snapshots, three solvent models (I–III) were tested.

I. The first "hybrid" (default) model, developed and tested in ref. [18], included clusters where water molecules closer than 3 Å to the sugar were kept, and the conductor-like continuum solvent model[36] was used for longer range solvation effects. The snapshots were partially optimized by performing 10 unrestrained optimization steps, and Raman and ROA spectral intensities calculated using the Gaussian program.[37] In the ONIOM electrostatic embedding[38] the sugar was described by the B3LYP[39]/6-311++G** level of theory, while Glycam[23] and TIP3P[40] molecular mechanics force fields were used for sugar/water, respectively.

II. In the "quantum mechanical" or QM" model, a lower B3LYP/6-31G** level of theory was used for the solvent; otherwise the same procedure and parameters were used as in the hybrid one, i.e. the sugar was described at the B3LYP/6-311++G** level. Before generation of the spectra, polarizability derivatives of water atoms were set to zero.
III. In the third "charges" model, no continuum was used for long range solvation effects but larger clusters with a 12 Å cutoff were made. They were optimized in a 10 steps optimization and for the final Raman/ROA calculations the water molecules were replaced by partial atomic charges only (TIP3P).

For the optimized clusters, harmonic Raman and ROA intensities were calculated[22,41] with Gaussian at the same level as for the optimization. For the third solvent model, anharmonic vibrational frequencies and intensities were calculated using the generalized second-order vibrational perturbation theory (GVPT2)[16,17] as implemented in Gaussian. Although the Fermi and Darling-Dennison resonances are partially included in GVPT2,[17] for about 20% of the clusters unreasonably big intensities were obtained (e.g., 1000-times larger than normal); these were ignored for the anharmonic computations.

Comparison of Theoretical and Experimental Spectra

From calculated Raman and ROA intensities of each band i (I_i), smooth spectra were constructed using Lorentzian shapes and a temperature factor[42] as [Eq. (1)]:

$$S(\omega) = \sum_i I_i \left[1 - \exp\left(-\frac{\omega_i}{kT}\right)\right]^{-1} \left[4\left(\frac{\omega - \omega_i}{\Delta}\right)^2 + 1\right]^{-1} \quad (1)$$

where ω_i is the transition frequency, k is the Boltzmann constant, T is temperature, and $\Delta = 7.5\ cm^{-1}$. In the fingerprint region (75–1700 cm^{-1}) the vibrational frequencies computed at the harmonic limit were multiplied by [Eqs. (2) and (3)]:

$$\phi(\omega) = a\left[1 + \exp\left(\frac{\omega_0 - \omega}{15}\right)\right]^{-1} + b\left\{1 - \left[1 + \exp\left(\frac{\omega_0 - \omega}{15}\right)\right]^{-1}\right\} \quad (2)$$

for $\omega < 2000\ cm^{-1}$ and by

$$\phi(\omega) = Q \quad (3)$$

for $\omega > 2000\ cm^{-1}$.

For the hybrid solvent model I, $\omega_0 = 1210\ cm^{-1}$, $a = 1$, $b = 0.978$, and $Q = 0.9575$. For model II, $\omega_0 = 1220\ cm^{-1}$, $a = 0.988$, $b = 0.974$, and $Q = 0.9540$. Previously, such a scaling allowed for an objective comparison of the simulated and experimental spectra in the fingerprint region.[18] In addition, factor Q was introduced for the CH stretching. The simulated and experimental curves were compared using relative overlap integrals[18] [Eq. (4)]:

$$\delta = \frac{\int S_{exp} S_{calc} d\omega}{\sqrt{\int S_{exp}^2 d\omega} \sqrt{\int S_{cal}^2 d\omega}} \quad (4)$$

where $S_{calc} = \sum c_i S_{calc,i}$, and the CH_2OH conformer ratios c_i were determined from MD simulations (Table 1).

Acknowledgements

The work was supported by the Czech Grant Agency, grants 20-10144S (P.B.), 18-05770S (J.K.) and 19-19561S (H.M-S., V.P.), and Ministry of Education, grants LTC17012, LM2015042, CERIT-SC, and LM2015085. We also acknowledge the European Regional Development Fund OP RDE (project ChemBioDrug no. CZ.02.1.01/0.0/0.0/16_019/0000729) and thank Pavel Jungwirth for the inspiring discussion on the topic.

Conflict of Interest

The authors declare no conflict of interest.

Keywords: CH stretching · density functional theory · Raman optical activity · saccharide structure · spectral modeling

[1] R. Politi, L. Sapir, D. Harries, *J. Phys. Chem. A* **2009**, *113*, 7548–7555.
[2] T. Fukuyama, K. Matsuo, K. Gekko, *Chirality* **2011**, *23*, E52–E58.
[3] P. K. Bose, P. L. Polavarapu, *Carbohyd. Res.* **1999**, *319*, 172–183.
[4] P. K. Bose, P. L. Polavarapu, *J. Am. Chem. Soc.* **1999**, *121*, 6094–6095.
[5] A. Melcerová, J. Kessler, P. Bouř, J. Kaminský, *Phys. Chem. Chem. Phys.* **2016**, *18*, 2130–2142.
[6] F. Zielinski, S. T. Mutter, C. Johannessen, E. W. Blanch, P. L. A. Popelier, *Phys. Chem. Chem .Phys.* **2015**, *17*, 21799–21809.
[7] J. R. Cheeseman, M. S. Shaik, P. L. A. Popelier, E. W. Blanch, *J. Am. Chem. Soc.* **2011**, *133*, 4991–4997.
[8] B. Mulloy, P. A. S. Mourão, E. Gray, *J. Biotechnology* **2000**, *77*, 123–135.
[9] M. Buděšínský, P. Daněček, L. Bednárová, J. Kapitán, V. Baumruk, P. Bouř, *J. Phys. Chem. A* **2008**, *112*, 8633–8640.
[10] L. Nafie, *Vibrational optical activity: Principles and applications*, Wiley, Chichester, **2011**.
[11] W. Hug, S. Kint, G. F. Bailey, J. R. Schere, *J. Am. Chem. Soc.* **1975**, *97*.
[12] J. Hudecová, V. Profant, P. Novotná, V. Baumruk, M. Urbanová, P. Bouř, *J. Chem. Theory Comput.* **2013**, *9*, 3096–3108.
[13] P. Michal, R. Čelechovský, M. Dudka, J. Kapitán, M. Vůjtek, M. Berešová, J. Šebestík, K. Thangavel, P. Bouř, *J. Phys. Chem. B* **2019**, *123*, 2147–2156.
[14] M. Hope, J. Šebestík, J. Kapitán, P. Bouř, *J. Phys. Chem. A* **2020**, *124*, 674–683.
[15] P. Carbonniere, T. Lucca, C. Pouchan, N. Rega, V. Barone, *J. Comput. Chem.* **2005**, *26*, 384–388.
[16] V. Barone, *J. Chem. Phys.* **2005**, *122*, 014108.
[17] J. Bloino, M. Biczysko, V. Barone, *J. Phys. Chem. A* **2015**, *119*, 11862–11874.
[18] V. Palivec, V. Kopecký, P. Jungwirth, P. Bouř, J. Kaminský, H. Martinez-Seara, *Phys Chem. Chem. Phys.* **2020**, *22*, 1983–1993.
[19] R. G. Nelson, W. C. Johnson, *J. Am. Chem. Soc.* **1976**, *98*, 4290–4295.
[20] W. Hug, *Appl. Spectrosc.* **2003**, *57*, 1–13.
[21] L. D. Barron, *Molecular Light Scattering and Optical Activity*, Cambridge University Press, Cambridge, UK, **2004**.
[22] J. R. Cheeseman, M. J. Frisch, *J. Chem. Theory Comput.* **2011**, *7*, 3323–3334.
[23] K. N. Kirschner, A. B. Yongye, S. M. Tschampel, J. González-Outeiriño, C. R. Daniels, B. L. Foley, R. J. Woods, *J. Comput. Chem.* **2008**, *29*, 622–655.
[24] F. Franks, P. J. Lillford, G. Robinson, *J. Chem. Soc., Faraday Trans. 1* **1989**, *85*, 2417–2426.
[25] W. Hug, G. Hangartner, *J. Raman Spectrosc.* **1999**, *30*, 841–852.
[26] P. Bouř, D. Michalík, J. Kapitán, *J. Chem. Phys.* **2005**, *122*, 144501.
[27] M. J. Abraham, T. Murtola, R. Schulz, S. Páll, J. C. Smith, B. Hess, E. Lindahl, *SoftwareX* **2015**, *1*, 19–25.
[28] W. G. Hoover, *Phys. Rev. A* **1985**, *31*, 1695–1697.
[29] M. Parrinello, A. Rahman, *J. Appl. Phys.* **1981**, *52*, 7182–7190.
[30] R. Danne, C. Poojari, H. Martinez-Seara, S. Rissanen, F. Lolicato, T. Róg, I. Vattulainen, *J. Chem. Inf. Model.* **2017**, *57*, 2401–2406.
[31] S. Izadi, A. V. Onufriev, *J. Chem. Phys.* **2016**, *145*, 074501.

[32] B. Hess, H. Bekker, H. J. C. Berendsen, J. G. E. M. Fraaije, *J. Comput. Chem.* **1997**, *18*, 1463–1472.
[33] T. Darden, Y. D. L. Pedersen, *J. Chem. Phys.* **1993**, *98*, 10089–10092.
[34] J. Jungwirth, J. Šebestík, M. Šafařík, J. Kapitán, P. Bouř, *J. Phys. Chem. B* **2017**, *121*, 8956–8964.
[35] Y. Zhu, J. Zajicek, A. S. Serianni, *J. Org. Chem.* **2001**, *66*, 6244–6251.
[36] A. Klamt, G. Schuurmann, *J. Chem. Soc., Perkin Trans. 2* **1993**, 799–805.
[37] M. J. Frisch, G. W. Trucks, H. B. Schlegel, G. E. Scuseria, M. A. Robb, J. R. Cheeseman, G. Scalmani, V. Barone, G. A. Petersson, H. Nakatsuji, X. Li, M. Caricato, A. V. Marenich, J. Bloino, B. G. Janesko, R. Gomperts, B. Mennucci, H. P. Hratchian, J. V. Ortiz, A. F. Izmaylov, J. L. Sonnenberg Williams, F. Ding, F. Lipparini, F. Egidi, J. Goings, B. Peng, A. Petrone, T. Henderson, D. Ranasinghe, V. G. Zakrzewski, J. Gao, N. Rega, G. Zheng, W. Liang, M. Hada, M. Ehara, K. Toyota, R. Fukuda, J. Hasegawa, M. Ishida, T. Nakajima, Y. Honda, O. Kitao, H. Nakai, T. Vreven, K. Throssell, J. A. Montgomery Jr., J. E. Peralta, F. Ogliaro, M. J. Bearpark, J. J. Heyd, E. N. Brothers, K. N. Kudin, V. N. Staroverov, T. A. Keith, R. Kobayashi, J. Normand, K. Raghavachari, A. P. Rendell, J. C. Burant, S. S. Iyengar, J. Tomasi, M. Cossi, J. M. Millam, M. Klene, C. Adamo, R. Cammi, J. W. Ochterski, R. L. Martin, K. Morokuma, O. Farkas, J. B. Foresman, D. J. Fox in *Gaussian 16 Rev. A.03*, Vol. (Ed. Eds.: Editor), City, **2016**.
[38] P. B. Karadakov, K. Morokuma, *Chem. Phys. Lett.* **1987**, *317*, 589–596.
[39] A. D. Becke, *J. Chem. Phys.* **1993**, *98*, 5648–5652.
[40] W. L. Jorgensen, J. Chandrasekhar, J. D. Madura, *J. Chem. Phys.* **1983**, *79*, 926–935.
[41] J. R. Cheeseman in *Calculation of Molecular Chiroptical Properties using Density Functional Theory*, (B. L. Feringa, W. Meijer, Eds.), University of Groningen, City, **2007**, pp. INV 3.
[42] P. L. Polavarapu, *Vibrational spectra: principles and applications with emphasis on optical activity*, Elsevier, Amsterdam, **1998**.

Manuscript received: March 30, 2020
Revised manuscript received: April 22, 2020
Accepted manuscript online: April 26, 2020
Version of record online: May 25, 2020